CHEMIJA. 2016. Vol. 27. No. 4. P. 192–201

Sol-gel derived calcium hydroxyapatite thin films on 316L stainless steel substrate: comparison of spin-coating and dip-coating techniques

V. Jonauskė*,

A. Prichodko,

R. Skaudžius,

A. Kareiva

Department of Inorganic Chemistry,
Faculty of Chemistry,
Vilnius University,
Naugarduko St. 24,
LT-03225 Vilnius, Lithuania

Aqueous sol-gel chemistry route has been developed to prepare nanostructured calcium hydroxyapatite ($Ca_{10}(PO_4)_6(OH)_2$; CHA) thin films on a 316L stainless steel substrate. In the sol-gel processing, calcium acetate monohydrate and phosphoric acid were used as Ca and P precursors, respectively. For the deposition of thin films spin-coating and dip-coating methods were used by coating the stainless steel substrate 5, 15 and 30 times in both cases. Each layer was consistently annealed at 850 °C in air. The obtained CHA coatings were examined using X-ray diffraction analysis (XRD), Fourier transform infrared spectroscopy (FTIR), scanning electron microscopy (SEM), atomic force microscopy (AFM) and contact angle measurements (CAM). The quality and specific features of CHA thin films obtained by spin- and dip-coating methods were compared in this study. It was demonstrated that both methods are suitable for the fabrication of CHA films on the 316L stainless steel substrate, however, the preference to the spin-coating technique could be given.

Keywords: biomaterials, ceramics, coatings, sol-gel growth

INTRODUCTION

Metallic implants such as 316L stainless steel, titanium and its alloys and cobalt chromium alloys have been widely used as implant materials in the recent years [1, 2]. The 316L stainless steel has gained a special attention among other metals and alloys due to its low cost, good mechanical properties and corrosion resistance. It has been widely used for orthopaedic, dental implants [3], and conventional spinal interbody fusion cages [4]. Additional applications include reconstructive surgery, heart valve parts, wire leads, and aneurysm clips [1]. When pure stainless steel is used in orthopaedic implants, osteo-integration does not occur and new tissue growth is not promoted [5]. With the purpose to improve the osteo-integration of 316L stainless steel, implants have been coated with calcium hydroxyapatite ($Ca_{10}(PO_4)_6(OH)_2$) (CHA) [6]. Poor mechanical properties of CHA limit application of this ceramic to little or no load bearing locations [7]. Therefore, pure CHA cannot be used in orthopaedic devices that must withstand substantial loadings during their expected lifetimes. To overcome this drawback, CHA has been applied as a thin coating on a metallic implant with the aim to combine the mechanical advantages of metals with the excellent biocompatibility of the ceramic [7–9]. Biocompatibility is defined as the ability of the device to continue performing the intended function, effectively and as long as necessary, in or on the body [1]. CHA due to its chemical and structural similarity to the human bone and teeth [9–11] permits cell adhesion, differentiation and proliferation [12, 13] and promotes bone ingrowth on the surface of the implant during the early stages of implantation [2, 8, 14]. Research has showed that use of CHA on a metallic implant can reduce the patient recovery time from 100 days with a non-coated implant to only 20 days with a CHA coated implant after the implantation [7]. CHA has been used commercially as a coating on metallic implants since the 1980s. CHA coatings on metallic substrates offer a great improvement in orthopaedic and dental applications and are used in successful clinical practices [15, 16]. A number of methods have been developed to apply CHA coatings on metallic implants such as sputtering, ion-beam deposition, electrophoretic deposition, high-velocity oxy-fuel spray (HVOF) [18], biomimetic deposition, wet precipitation [16], electro-deposition, laser ablation, sol-gel, plasma spraying [17, 19]. Plasma spraying is the most popular technique used commercially and the only clinically accepted method to deposit CHA [2, 6]. However, it has significant disadvantages such as poor control over coating

* Corresponding author. E-mail: vilma.ciuvasovaite@gmail.com

phase composition, crystallinity, thickness, morphology, and resistance to delamination [14, 18, 20]. Even more, the plasma spraying method requires extremely high temperatures and expensive equipment [21]. The sol-gel technique, being one of the thin film fabrication methods, provides some benefits over the plasma spraying method, such as the chemical homogeneity and fine grain structure of the end product, and low processing temperature. Moreover, compared with other thin film methods, the sol-gel method is simple and cost-efficient, effective for the coating of complex-shaped materials and can be carried out under low temperatures [22, 23]. In this work we have focused on the development of an aqueous sol-gel synthesis processing for the fabrication of CHA coatings on the 316L stainless steel substrate. The comparison of suitability of two techniques, namely dip-coating and spin-coating, for the preparation of CHA thin films is also discussed.

EXPERIMENTAL

Calcium acetate monohydrate ($Ca(CH_3COO)_2 \cdot H_2O$; 99.9%; Fluka) and phosphoric acid (H_3PO_4; 85.0%; Reachem) were used as starting materials for the synthesis of CHA coatings, respectively. 5.2854 g (0.03 mol) of calcium acetate monohydrate were dissolved in 40 ml of distilled water and mixed with 4 ml of complexing agent 1,2-ethanediol (99.0%; Alfa Aesar). To this solution, 9.6439 g (0.033 mol) of ethylenediaminetetraacetic acid (EDTA; 99.0%; Alfa Aesar) deprotonated with 24 ml of triethanolamine (99.0%; Merck) were slowly added. After 10 h of stirring, 1.23 ml of phosphoric acid diluted with 20 ml of distilled water were added to the solution. After stirring for 24 h, 25 ml of the obtained gel were mixed with 15 ml of 3% polyvinyl alcohol (PVA7200, 99.5%; Aldrich). The obtained solution was stirred in a beaker covered with watch glass at room temperature and was used for the coating of commercial 316L stainless steel substrates (rectangular plates of $20 \times 10 \times 0.5$ mm were used for dip-coating and circle plates of 20 mm diameter for spin-coating). The surface of stainless steel plates were roughened with sandpaper, cleaned with acetone in an ultrasonic cleaner for 15 minutes and then air dried. Dip-coating and spin-coating techniques were employed to produce CHA coatings. Stainless steel rectangles were dip-coated in the sol solution with appropriate immersing (85 mm/min) and withdrawal (40 mm/min) rates. For the spin-coating procedure, approximately 0.5 ml of the coating solution was placed on the top of the substrate using a syringe and then spin coated at 2000 RPM for 60 s in air. Both rectangle and circle substrates were repeatedly coated 5, 15 and 30 times following the same procedures accordingly and each time annealed at 850 °C for 5 h in an oven. X-ray diffraction analysis (XRD) was performed on a Bruker AXE D8 Focus diffractometer with a LynxEye detector using CuKa radiation. The changes of the layers were evaluated by Fourier transform infrared spectroscopy (FTIR) using a Perkin-Elmer FTIR Spectrum BX II spectrometer. The microstructure and morphology of the obtained samples were investigated using a Hitachi SU-70 scanning electron microscope (SEM) and a BioScope Catalyst atomic force microscope (AFM). For the evaluation of hydrophobicity of the CHA coatings the contact angle measurements (KVS Instrument CAM 100) were performed.

RESULTS AND DISCUSSION

The phase composition of the coatings was determined by XRD analysis. Figure 1 shows the diffraction patterns of CHA

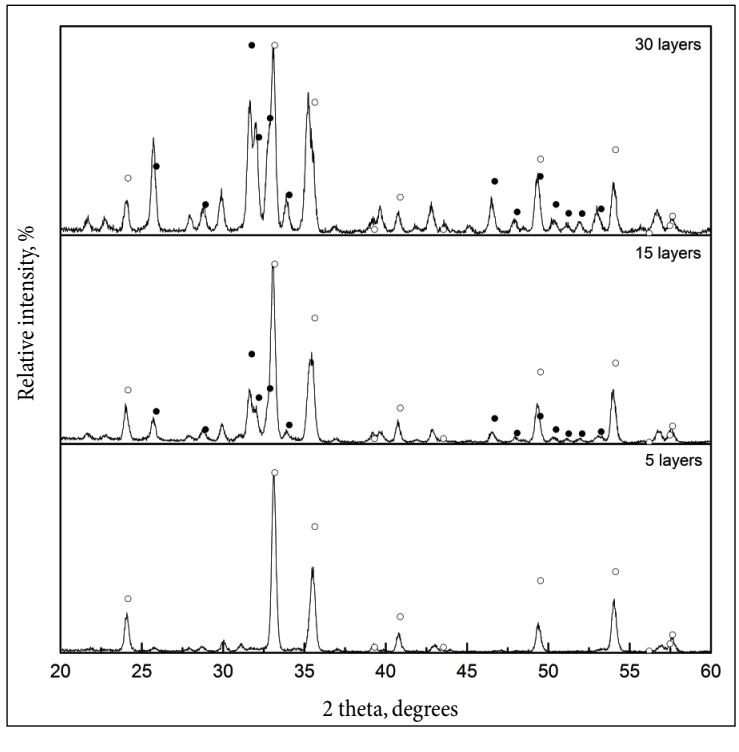

Fig. 1. XRD patterns of C-P-O gels annealed at 850 °C for 5 h after 5, 15 and 30 spinning procedures. Diffraction peaks are marked: ● is $Ca_{10}(PO_4)_6OH_2$, ○ is Fe_2O_3

films synthesized using the spin-coating technique. The influence of the spinning and annealing procedures on the formation of the CHA phase is clearly seen. After five spinning and annealing procedures the only phase of Fe_2O_3 ($2\theta \approx 24.5$, 33.5, 35.2 and 41.5; ICSD [033-0664]) could be determined. As seen from Fig. 1, the formation of the CHA phase ($2\theta \approx 31.8$; PDF [9-432]) started after repeating the spinning and annealing procedure for 15 times. However, the Fe_2O_3 phase remained as a dominant phase. Diffraction peaks attributable to CHA are well resolved and intensive in the sample obtained after 30 spin-coating procedures. Very similar results were obtained for the preparation of CHA thin films using the dip-coating method (see Fig. 2). The intensity of diffraction lines attributable to the $Ca_{10}(PO_4)_6(OH)_2$ phase increases with increasing the time of spinning and annealing procedures. From the XRD measurements we can conclude that both spin-coating and dip-coating techniques are suitable for the fabrication of CHA on the surface of stainless steel.The FTIR spectra of the sol-gel derived CHA coatings obtained by spin- and dip-coating procedures are shown in Figs. 3 and 4, respectively. The characteristic absorption lines of the P-O vibrations in PO_4^{3-} ($Ca_{10}(PO_4)_6(OH)_2$) in a range of 1100–950 cm^{-1} are clearly visible in both spin-coated and dip-coated samples obtained after 15 coating and annealing procedures [24, 25]. The broad band ranging from 3600 to 3300 cm^{-1} can be attributed to the O-H

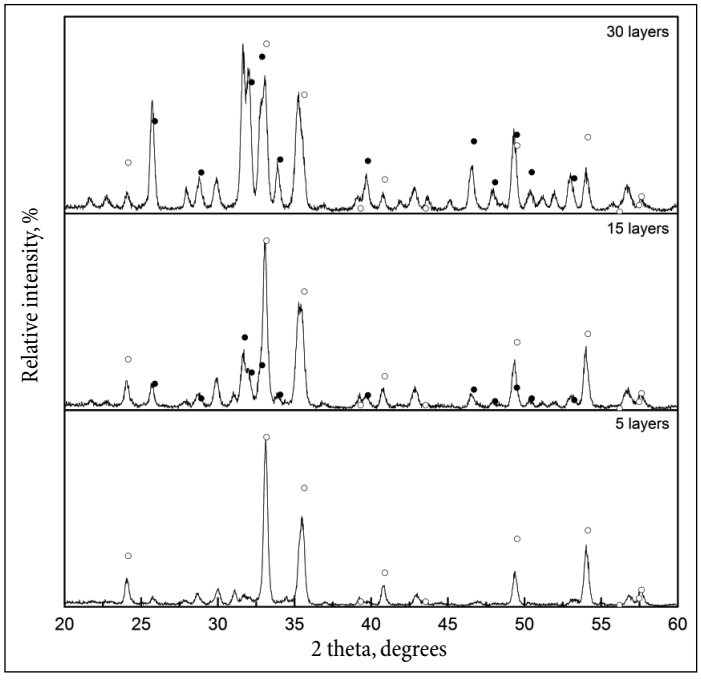

Fig. 2. XRD patterns of C-P-O gels annealed at 850 °C for 5 h after 5, 15 and 30 dipping procedures. Diffraction peaks are marked: ● is $Ca_{10}(PO_4)_6OH_2$, ○ is Fe_2O_3

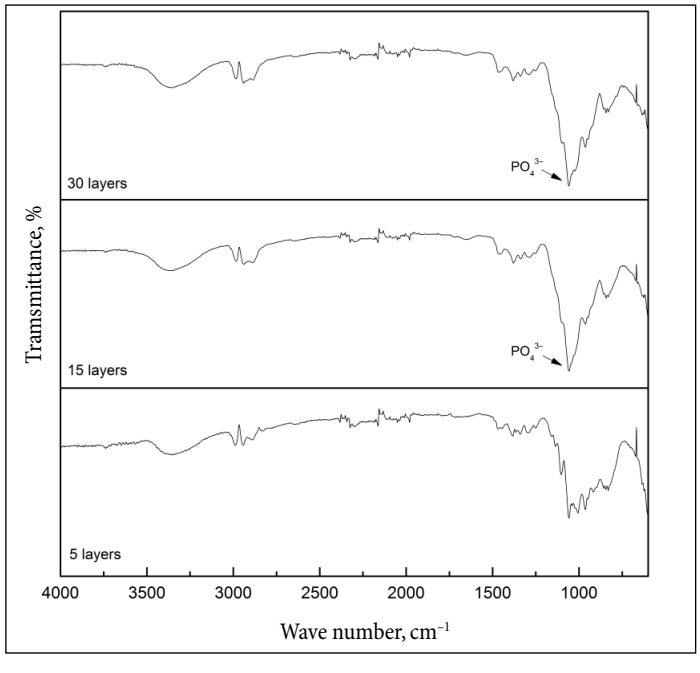

Fig. 3. FTIR spectra of C-P-O gels annealed at 850 °C for 5 h after 5, 15 and 30 spinning procedures

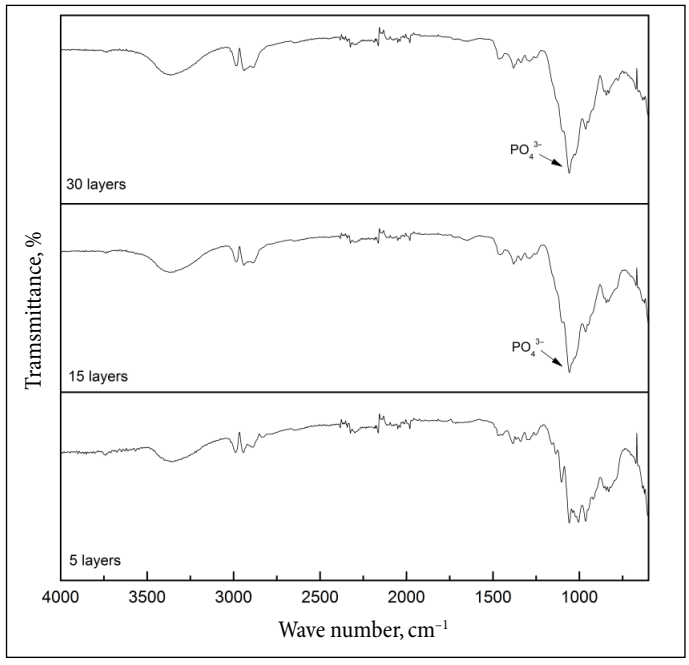

Fig. 4. FTIR spectra of C-P-O gels annealed at 850 °C for 5 h after 5, 15 and 30 dipping procedures

vibration of adsorbed water during the exposure of dried samples to air [26]. The bands visible at 2350 cm^{-1} belong to carbon dioxide from atmosphere [27]. Similarity of the FTIR spectra of spin-coated and dip-coated samples is in a good agreement with the XRD results and confirms that both deposition techniques can be successfully applied to prepare CHA thin films on stainless steel. The surface morphological properties of the synthesized CHA coatings were investigated using scanning electron microscopy (SEM) and atomic force microscopy (AFM). The SEM micrographs of the 316L stainless steel plate treated with sandpaper and obtained at different magnification are shown in Fig. 5. As seen, the surface of the substrate is very rough and composed of pyramidal crystallites. Figure 6 represents the SEM micrographs of both samples containing 5 layers of precursor gel and heated at 850 °C. The SEM images clearly differ from the substrate micrographs. It seems that the steel substrate after the spin-coating procedure is more evenly coated with the product. In comparison, the network of irregularly shaped particles (probably, iron oxide) could be observed in the SEM micrograph of the dip-coated sample. The SEM images of the samples containing 15 layers of CHA and obtained at different magnification are presented in Fig. 7. The both steel surfaces are homogenously coated by calcium hydroxyapatite showing a porous microstructure. However, the changes in the surface morphology of differently prepared CHA samples are visible. Interestingly, the surface quality after 15 procedures is slightly better of the CHA sample obtained via dip-coating. As seen, the synthesized film using the dip-coating technique is composed of evenly distributed spherical particles less than 200 nm in size with high connectivity between grains. Figure 8 shows the SEM micrographs of CHA thin films obtained after 30 coating and annealing procedures.

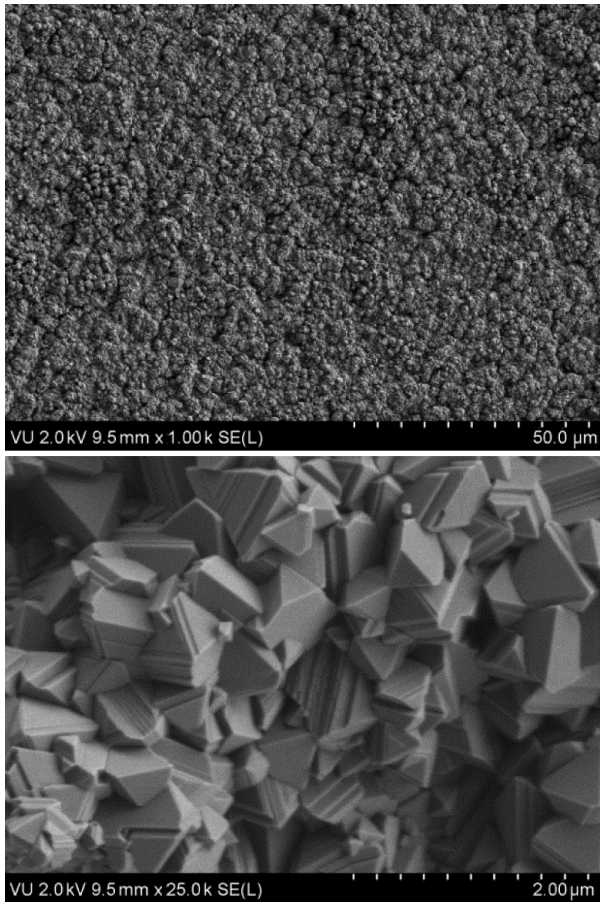

Fig. 5. SEM micrographs of the 316L stainless steel substrate treated with sandpaper and obtained at different magnification

The coatings appear uniform, crack free and completely cover substrates. At higher magnification the SEM images indicated a different surface morphology of spin- and

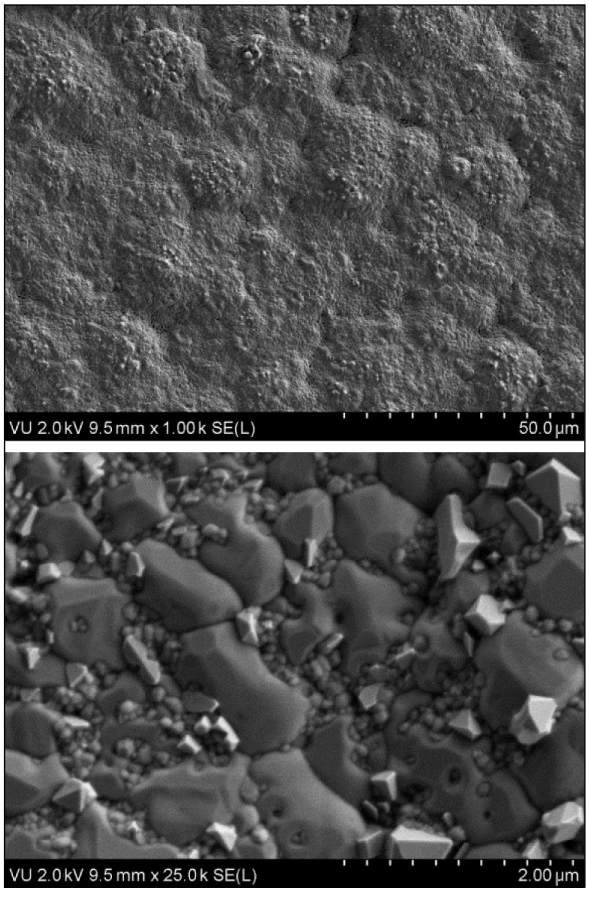

Fig. 6. SEM micrographs of CHA samples containing 5 layers and obtained by spin-coating (at left) and dip-coating (at right) techniques

dip-coated samples. The SEM image of the spin-coated sample is homogeneous and composed of nano-scaled particles. The individual particles are about 100–300 nm in size. These particles appear to have fused together to form stone-like deposits [28]. Interestingly, the dip-coated sample is not fully dense and remains porous with a coral structure. The pores appear to be of a nano-scale size range. The SEM results showed that despite the structural similarities of the coatings, morphological changes were affected by the coating technique. With both preparation techniques the stainless steel substrates were fully covered by CHA, despite different texture of thin films obtained. CHA with a coral structure has a considerable success considering its porous structure. It is similar to the human cancellous bone and the material could form chemical bonds with the bone and soft tissue *in vivo* [29]. Such type of implants show enhanced biological interactions and hence accelerate fixation to the bone [29, 30]. *In vitro* tests of the CHA coatings with a homogeneous particle distribution also revealed the chemical reaction of particles with the surrounding body fluid, considered as a signal of bioactivity [31]. Additionally, the dense CHA ceramic exhibits a higher fracture toughness having improved mechanical properties [32, 33]. Moreover, both samples appear to be good candidates for biocompatible drug carriers, since they can be resorbed by

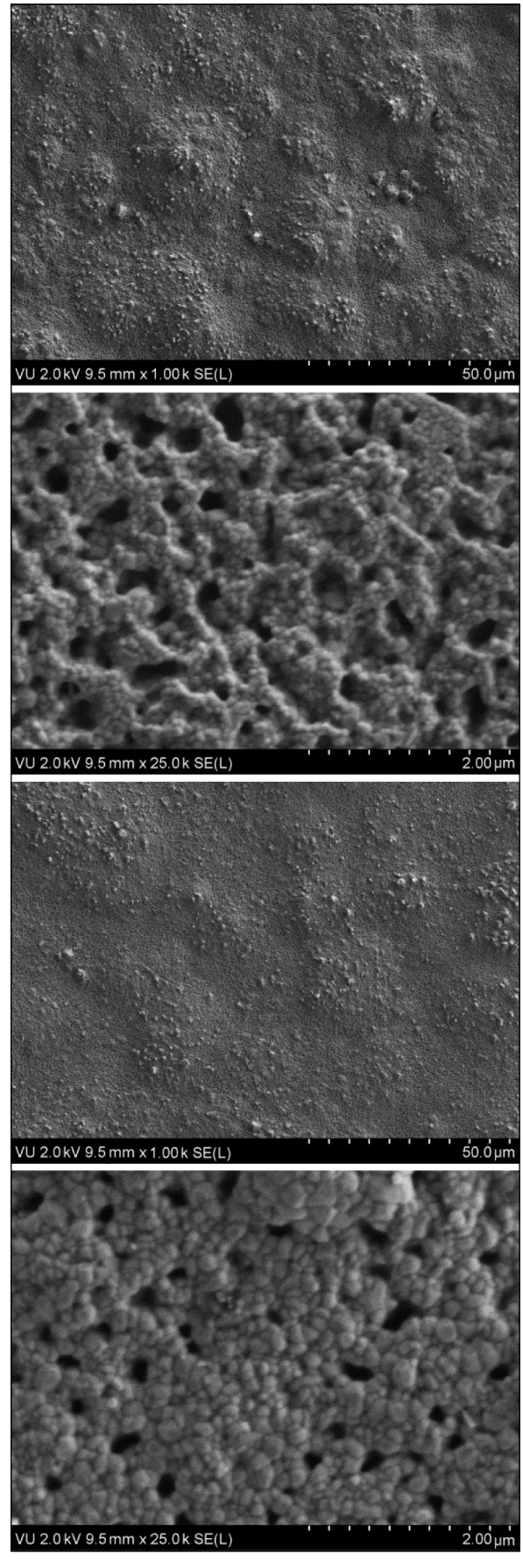

Fig. 7. SEM micrographs of CHA samples containing 15 layers and obtained by spin-coating (at top) and dip-coating (at bottom) techniques

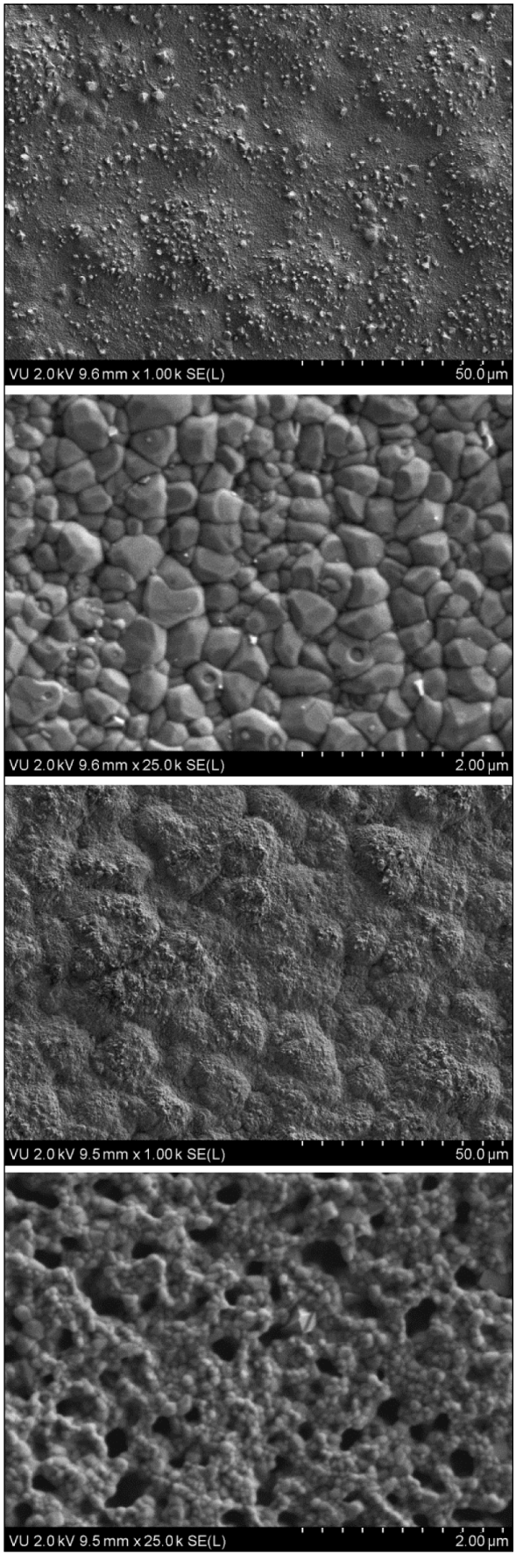

Fig. 8. SEM micrographs of CHA samples containing 30 layers and obtained by spin-coating (at top) and dip-coating (at bottom) techniques

cells and promote new bone formation [34–36]. Atomic force microscopy (AFM) was also used as an additional tool to investigate the surface morphology of the CHA coatings. The AFM images of the uncoated substrate and CHA coatings are shown in Figs. 9–12. The AFM 3D images of different areas of the prepared stainless steel substrate are presented in Fig. 9. As shown, the stainless steel substrate used in our experiments revealed micro-scale topography. As was mentioned earlier, the surface of the substrate is not atomically smooth. In Fig. 10 the AFM 3D images of the films containing 5 layers of the Ca-P-O gel deposited by spin- and dip-coating techniques are presented. Again, the AFM images clearly differ from the substrate images. The AFM topographs show a network of crystallites with intercrystalline vacant spaces [37]. However, the AFM images do not show differences in the topography between the synthesized samples using different techniques. The surfaces are rough and contain similar bumps. The AFM images of the specimens containing 15 and 30 layers are slightly different. The AFM 3D surface topology of the samples containing 15 layers of CHA and obtained by different techniques is presented in Fig. 11. These images exhibit a homogeneous coverage of the CHA coating on the surface of the substrate [38]. Apparently, the coating increased the surface texture of the sample which is in a good agreement with the SEM results. The surface of the CHA films containing 30 layers is smooth with larger crystals and a more homogeneous crystal size distribution. The AFM results of surface roughness measurements for the CHA films are presented

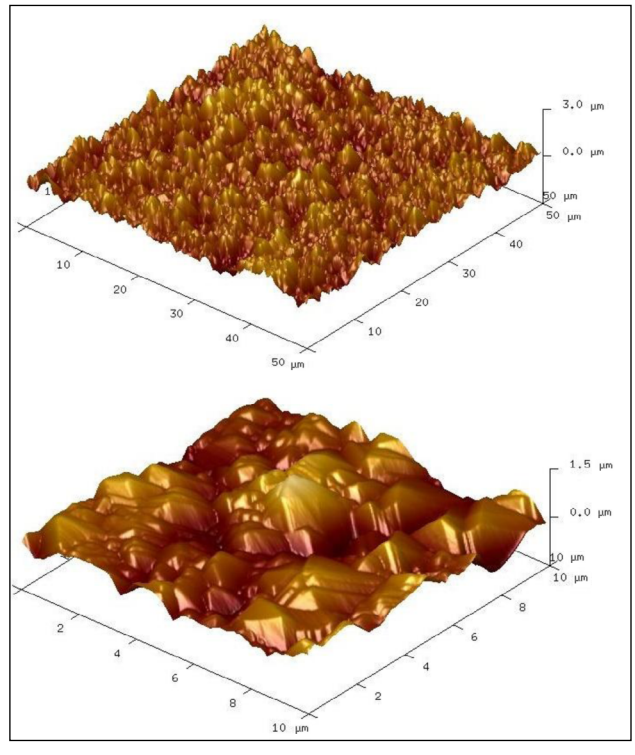

Fig. 9. AFM images of different areas of the prepared stainless steel substrate

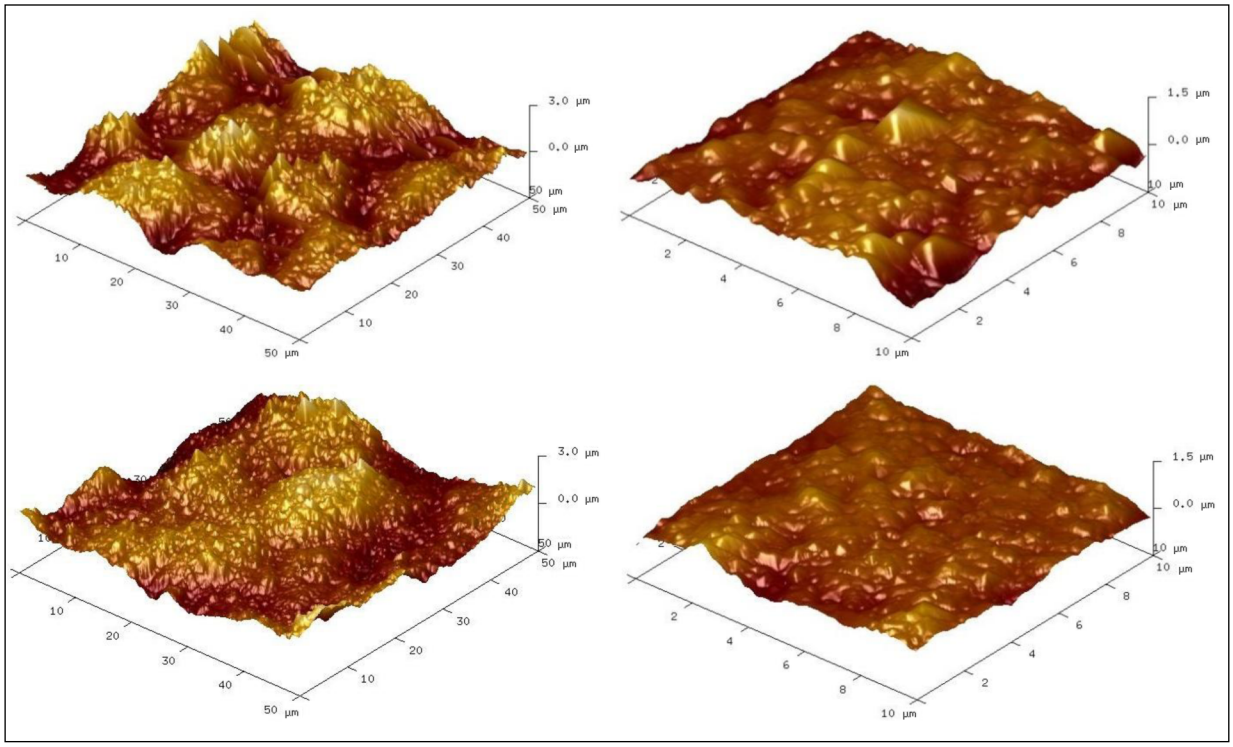

Fig. 10. AFM images of different areas of the samples containing 5 layers of C-P-O gel deposited by spin-coating (at top) and dip-coating (at bottom) techniques

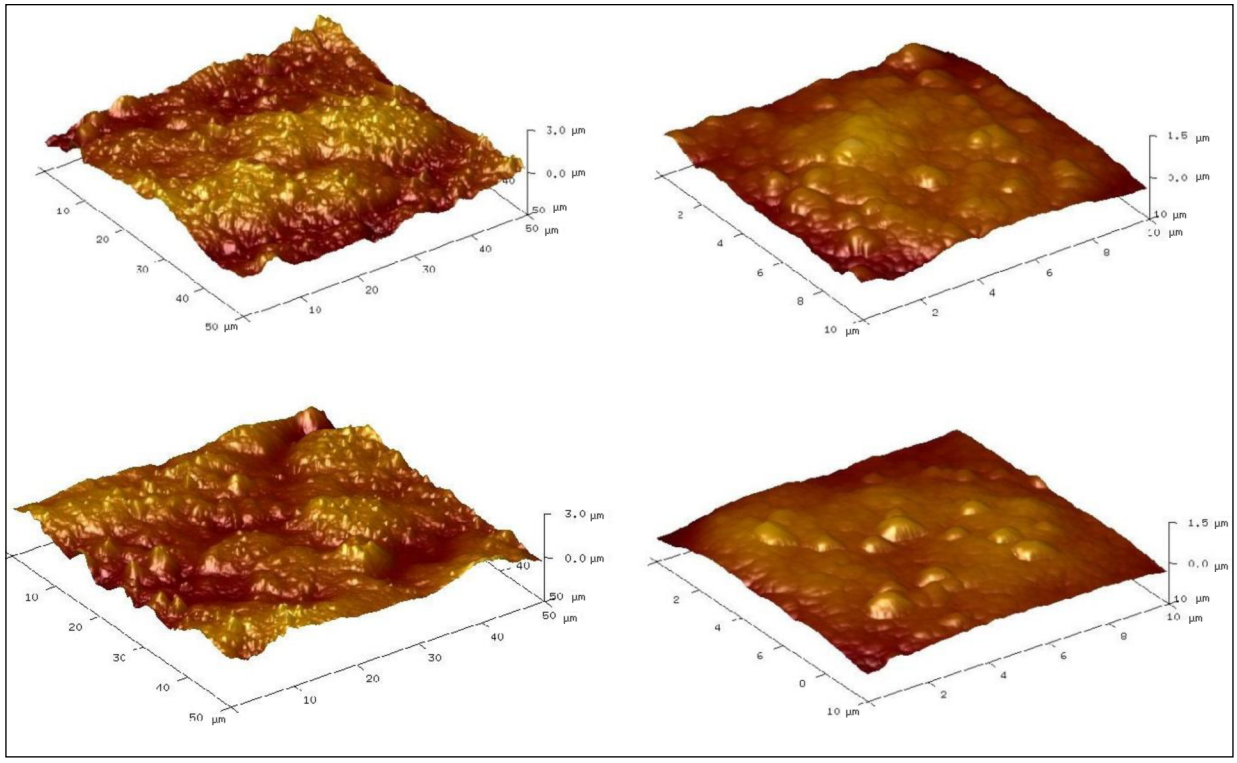

Fig. 11. AFM images of different areas of samples containing 15 layers of C-P-O gel deposited by spin-coating (at top) and dip-coating (at bottom) techniques

in Table 1. As seen from Table 1, the roughness of the stainless steel substrate after five spinning and annealing procedures has changed negligibly. This is related with the fact that only the crystalline phase of Fe_2O_3 was determined in these samples. The roughness of CHA films remains almost the same with an increasing number of layers from 15 to 30 by both spin- and dip-coating techniques. The AFM results suggested that the surface roughness and morphology of

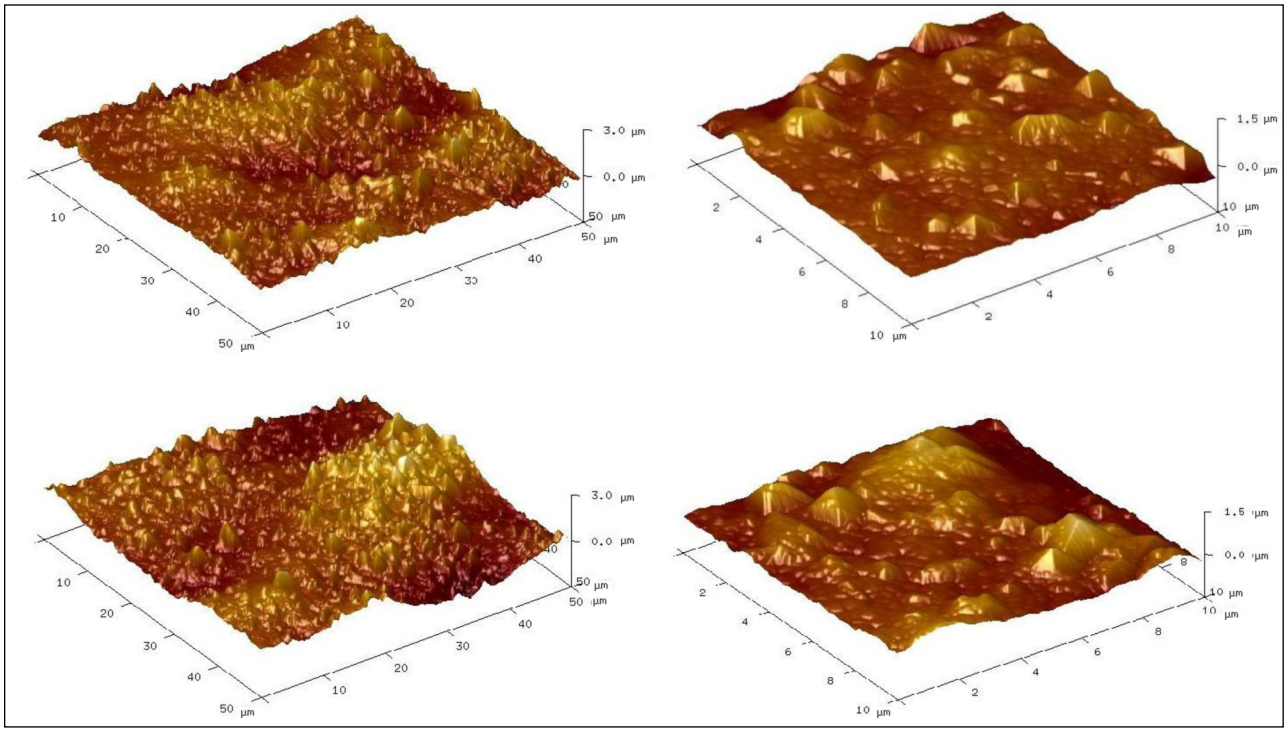

Fig. 12. AFM images of different areas of samples containing 30 layers of C-P-O gel deposited by spin-coating (at top) and dip-coating (at bottom) techniques

Table 1. **The AFM results of surface roughness measurements for CHA films obtained using different techniques**

Number of layers	RMS (Rq, nm)			
	Surface area 10/10 μm		Surface area 50/50 μm	
	Spin-coating	Dip-coating	Spin-coating	Dip-coating
0	37.9		40.2	
5	37.8	34.9	56.3	44.4
15	29.7	30.1	38.8	39.8
30	28.0	27.3	36.9	37.1

the CHA films changed remarkably in comparison with the uncoated substrate. Moreover, the presence of smaller grains along the step-edges (see Fig. 12) proves the presence of considerable grain mobility during the deposition process [39]. Contact angle measurements (CAM) were performed to estimate the hydrophobic and hydrophilic properties of CHA coatings. The results of these analyses are presented in Fig. 13. The contact angle value determined for the stainless steel substrate was 107.3. Interestingly, the wettability of CHA coatings depends on a number of layers of the samples obtained both by dipping and spinning techniques. The contact angle of dip-coated samples decreased from 78.6 up to 69.0 with increasing the amount of layers from 15 to 30. However, the spin-coated sample had different tendency in the change of the contact angle. The contact angle of spin-coated samples increased from 56.4 up to 78.8 with increasing the amount of layers from 15 to 30. The coatings obtained using both spin- and dip-coating techniques were hydrophilic which is in a good

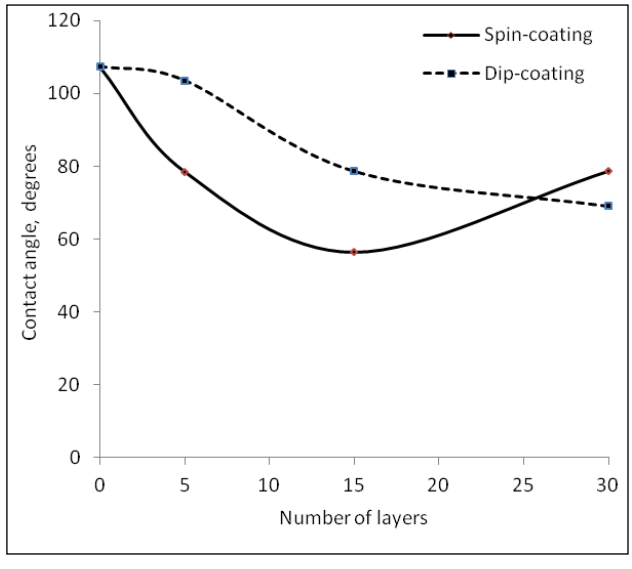

Fig. 13. The results of contact angle measurements

agreement with previously published results [40]. Moreover, the increased hydrophilicity of the CHA coated stainless steel compared to the uncoated stainless steel was determined. Hence, the CHA coated stainless steel with enhanced wettability can accelerate osseointegration, i. e. a structural and functional connection between the living bone and the surface of a load-bearing artificial implant [41]. The results obtained in this study could be considered of the primary interest since sol-gel processing allows the deposition of CHA of different morphology on complex substrates, which are constantly required in dental and orthopaedic applications. Moreover, repairing of large bone defects by the techniques described in this study is possible [42, 43].

CONCLUSIONS

The aqueous sol-gel method was developed for the synthesis of calcium hydroxyapatite (CHA) thin films on the stainless steel substrate. Hydroxyapatite biocoatings were fabricated using two different deposition techniques: dip-coating and spin-coating. A direct comparison of the CHA films obtained using different techniques was made in this work. The XRD and FTIR results revealed that the formation of CHA is directly influenced by the number of the C-P-O precursor gel layers applying both preparation techniques. The intensity of diffraction lines attributable to the $Ca_{10}(PO_4)_6(OH)_2$ phase increased with increasing the time of spinning or dipping and annealing procedures. From these measurements we concluded that both spin-coating and dip-coating techniques are suitable for the fabrication of CHA on the surface of stainless steel. The main morphological features of CHA films obtained by dip- and spin-coating techniques were investigated by SEM and AFM. The SEM results showed that despite the structural similarities of coatings, the morphological features were affected by the coating technique. The spin-coated CHA sample was homogeneous and composed of nano-scaled particles with individual particles about 100–300 nm in size. The dip-coated CHA coating was not fully dense and was porous with a coral structure. The AFM results suggested that the surface roughness and morphology of the CHA films changed remarkably in comparison with the uncoated substrate. Moreover, the presence of smaller grains along the step-edges suggested the presence of considerable grain mobility during the deposition process. The CHA coated stainless steel showed enhanced wettability which can accelerate the functional connection between the living bone and the surface of an artificial implant.

ACKNOWLEDGEMENTS

The financial support to A. P. from the Research Council of Lithuania under Project "Postdoctoral Fellowship Implementation in Lithuania" (No. 004/102) is greatly acknowledged. This research was also partially funded by COST Action MP1202.

Received 25 July 2016
Accepted 7 September 2016

References

1. I. Gurappa, *Surf. Coat. Tech.*, **161**, 70 (2002).
2. D. Gopi, J. Indira, *Surf. Coat. Tech.*, **206**, 2859 (2012).
3. D. Gopi, S. Ramya, D. Rajeswari, M. Surendiran, L. Kavitha, *Colloids Surf., B*, **114**, 234 (2014).
4. B. D. Hahn, D. S. Park, J. J. Choi, et al., *Appl. Surf. Sci.*, **283**, 6 (2013).
5. L. Hao, S. Dadbakhsh, O. Seaman, M. Felstead, *J. Mater. Process. Technol.*, **209**, 5793 (2009).
6. C. P. O. Ossa, S. O. Rogero, A. P. Tschiptschin, *J. Mater. Sci.: Mater. Med.*, **17**, 1095 (2006).
7. D. M. Liu, Q. Yang, T. Troczynski, *Biomaterials*, **23**, 691 (2002).
8. L. Duta, F. N. Oktar, G. E. Stan, et. al., *Appl. Surf. Sci.*, **265**, 41 (2013).
9. M. Javidi, S. Javadpour, M. E. Bahrololoom, J. Ma, *Mater. Sci. Eng.*, C, **28**, 1509 (2008).
10. G. A. Fielding, M. Roy, A. Bandyopadhyay, S. Bose, *Acta Biomater.*, **8**, 3144 (2012).
11. D. T. M. Thanh, P. T. Nam, N. T. Phuong, et al., *Mater. Sci. Eng.*, C, **33**, 2037 (2013).
12. H. Wang, Y. Li, Y. Zuo, J. Li, S. Ma, L. Cheng, *Biomaterials*, **28**, 3338 (2007).
13. H. Zhou, J. Lee, *Acta Biomater.*, **7**, 2769 (2011).
14. B. D. Hahn, J. M. Lee, D. S. Park, J. J. Choi, J. Ryu, *Thin Solid Films*, **519**, 8085 (2011).
15. E. Mohseni, E. Zalnezhad, A. R. Bushroa, *Int. J. Adhes. Adhes.*, **48**, 238 (2014).
16. D. M. Liu, T. Troczynski, W. J. Tseng, *Biomaterials*, **22**, 1721 (2001).
17. H. Khandelwal, G. Singh, K. Agrawal, S. Prakash, R. D. Agarwal, *Appl. Surf. Sci.*, **265**, 30 (2013).
18. J. N. Barry, B. Twomey, A. Cowley, L. O'Neill, P. J. McNally, D. P. Dowling, *Surf. Coat. Tech.*, **226**, 82 (2013).
19. D. Gopi, V. Collins, A. Prakash, et al., *Corros. Sci.*, **53**, 2328 (2011).
20. P. Peng, S. Kumar, N. H. Voelcker, E. Szili, R. St. C. Smart, H.J. Griesser, *J. Biomed. Mater. Res., A*, **76**, 347 (2006).
21. D. de Souza, M. A. E. Cruz, A. N. De Faria, D. C. Zancanela, A. M. S. Simão, *Colloids Surf., B*, **118**, 31 (2014).
22. T. Oldinga, M. Sayera, D. Barrow, *Thin Solid Films*, **398–399**, 581 (2001).
23. C. J. Tredwin, A. M. Young, G. Georgiou, S. H. Shin, H. W. Kim, J. C. Knowles, *Dent. Mater. J.*, **29**, 166 (2013).
24. A. Epiphanova, O. Magaev, O. Vodyankina, *J. Sol-Gel Sci. Technol.*, **61**, 509 (2012).
25. E. Garškaitė, K. A. Gross, S. W. Yang, Thomas C. K. Yang, J. C. Yang, A. Kareiva, *Cryst. Eng. Comm.*, **16**, 3950 (2014).

26. I. Bogdanovičienė, A. Beganskienė, A. Kareiva, et al., *Chemija*, **21**, 98 (2010).
27. N. Dubnikova, E. Garškaitė, A. Beganskienė, A. Kareiva, *Opt. Mater.*, **33**, 1179 (2011).
28. L. Gan, R. Pilliar, *Biomaterials*, **25**, 5303 (2004).
29. A. H. Choi, B. Ben-Nissan, *Nanomedicine*, **2**, 51 (2007).
30 O. M. Goudouri, E. Kontonosaki, A. Theocharidou, et al., *Mater. Chem. Phys.*, **125**, 309 (2011).
31. C. Garcia, S. Cere, A. Duran, *J. Non-Cryst. Solids*, **348**, 218 (2004).
32. A. C. Tas, *J. Am. Ceram. Soc.*, **84**, 295 (2001).
33. H. Y. Yasuda, S. Mahara, T. Nishiyama, Y. Umakoshi, *Sci. Tech. Adv. Mater.*, **3**, 29 (2002).
34. S. Josse, C. Faucheux, A. Soueidan, et al., *Adv. Mater.*, **16**, 1423 (2004).
35. W. D. Zhang, Y. M. Chai, X. H. Xu, Y. L. Wang, N. N. Cao, *Appl. Surf. Sci.*, **322**, 71 (2014).
36. J. S. Son, T. Y. Kwon, K. H. Kim, *J. Nanosci. Nanotechnol.*, **15**, 130 (2015).
37. S. S. Kamble, A. Sikora, S. T. Pawar, N. N. Maldar, L. P. Deshmukh, *J. Alloys Compd.*, **623**, 466 (2015).
38. S. Hosseini, H. Naderi-Manesh, H. Vali, S. Faghihi, *Mater. Chem. Phys.*, **143**, 1364 (2014).
39. M. A. Surmeneva, R. A. Surmenev, A. I. Tyurin, et al., *Thin Solid Films*, **571**, 218 (2014).
40. M. Malakauskaitė-Petrulevičienė, Ž. Stankevičiūtė, A. Beganskienė, A. Kareiva, *J. Sol-Gel Sci. Technol.*, **71**, 437 (2014).
41. S. Anne Pauline, N. Rajendran, *Appl. Surf. Sci.*, **290**, 448 (2014).
42. M. Manso-Silvan, M. Langlet, C. Jimenez, M. Fernandez, J. M. Martinez-Duart, *J. Eur. Ceram. Soc.*, **23**, 243 (2003).
43. N. Harada, Y. Watanabe, K. Sato, et. al., *Biomaterials*, **35**, 7800 (2014).

V. Jonauskė, A. Prichodko, R. Skaudžius, A. Kareiva

KALCIO HIDROKSIAPATITO PLONI SLUOKSNIAI, SUSINTETINTI ZOLIŲ-GELIŲ BŪDU ANT 316L NERŪDIJANČIO PLIENO: SUKIMO IR MERKIMO DENGIMO METODŲ PALYGINIMAS

S a n t r a u k a

Sukurtas vandeninis zolių-gelių metodas plonų kalcio hidroksiapatito plėvelių ($Ca_{10}(PO_4)_6(OH)_2$) nusodinimui ant nerūdijančio plieno 316L pagrindo. Pradinėmis medžiagomis naudojant kalcio acetato monohidratą ir fosforo rūgštį atitinkamai gauti Ca ir P jonai. Plonos plėvelės gautos taikant sukimo ir merkimo metodus, plieninį pagrindą dengiant 5, 15 ir 30 kartų. Kiekvienas sluoksnis buvo kaitinamas 850 °C ore. Gautų dangų ištyrimui taikyta rentgeno difrakcinė analizė, infraraudonųjų spindulių spektroskopija, skenuojanti elektroninė mikroskopija, atominės jėgos mikroskopija ir kontaktinio kampo matavimas. Šiame straipsnyje palyginami sukimo ir merkimo metodai, aprašomos gautų kalcio hidroksiapatito plonų dangų savybės. Parodyta, kad abu metodai tinkami plonoms kalcio hidroksiapatito dangoms formuoti ant nerūdijančio plieno 316L pagrindo, tačiau pirmenybė galėtų būti teikiama sukimo metodui.